

Article

Effect of Baffle Board on Aerodynamic and Stealth Performance of Double S-Duct Caret Intake

Bin Wang , Qiang Wang and Sichen Li

School of Energy and Power Engineering, Beihang University, Beijing 100191, China; qwang518@buaa.edu.cn (Q.W.); buaasepe_lsc@buaa.edu.cn (S.L.)

* Correspondence: jijj16611@163.com

Abstract: Intake is not only the main air supply component of an aircraft, but also one of the forward radar scattering sources. The aerodynamic and stealth performance of intake is critical to the serviceability of advanced fighter aircrafts. The effects of baffle boards with different configurations on the performance of the caret intake with a double S-duct diffuser are presented in this article. The multi-level fast multipole method (MLFMM) and the SST $k-\omega$ turbulence model were respectively used to calculate the surface current and the flow field. It was found that the average RCS value of intake can be effectively reduced by installing the baffle board with vertical orientation in the front diffuser, with the DC60 value and the loss of outlet total pressure both increased slightly. The boundary layer separation and the RCS characteristics of intake were closely related to the configuration of the corrugated baffle board. Compared with the traditional curved board, by installing the corrugated board with optimized corrugation number and shape, the stealth performance of intake can be further improved, and the loss of aerodynamic performance can be also reduced.

Keywords: double S-duct caret intake; curved baffle board; corrugated baffle board; total pressure recovery; radar cross-section



Citation: Wang, B.; Wang, Q.; Li, S. Effect of Baffle Board on Aerodynamic and Stealth Performance of Double S-Duct Caret Intake. *Appl. Sci.* **2024**, *14*, 3747. <https://doi.org/10.3390/app14093747>

Academic Editor: Francesca Scargiali

Received: 25 February 2024

Revised: 11 April 2024

Accepted: 24 April 2024

Published: 27 April 2024



Copyright: © 2024 by the authors. Licensee MDPI, Basel, Switzerland. This article is an open access article distributed under the terms and conditions of the Creative Commons Attribution (CC BY) license (<https://creativecommons.org/licenses/by/4.0/>).

1. Introduction

A non-significant RCS value plays a very important role in the safety of an advanced fighter. It has been proven that the forward radar echo intensity of an aircraft could be significantly influenced by the intake [1]. Therefore, understanding how to effectively reduce the influence of intake on the RCS characteristics of a fighter is very important. The compression section of the caret intake is designed according to the waverider principle [2] and has an uncomplicated structure, with excellent aerodynamic performance [3] and non-significant RCS characteristics. Therefore, the caret intake is highly applicable for use in advanced stealth fighters.

By using computing technologies and a variety of suitable turbulence models, the efficiency and precision of computational fluid dynamics (CFD) methods in simulating the complex flow field of intake have been fully developed [4–6]. Therefore, in addition to experimental methods [7], CFD methods have become another common approach for analyzing the aerodynamic performance of intake. Shu [8] used a field velocity method to numerically simulate the flow field of a serpentine intake exposed to non-stationary horizontal sinusoidal gusts, and proved that the gusts could cause the deterioration of outlet distortion. Rajan [9] used the SST $k-\omega$ turbulence model to investigate the aerodynamic performance of a supersonic intake, and proved that the boundary layer bleed could reduce the outlet distortion. Javad [10] simulated the airflow field of a supersonic intake by using the SST $k-\omega$ model, and proved that the interaction between the shock wave and the boundary layer could be the main reason for the buzz onset.

In radar stealth research, the larger the RCS value of the object, the stronger the scattered radar echo intensity, and the worse the stealth performance. According to the

finite element method, the RCS value can be investigated by obtaining the surface current, and a variety of computational electromagnetic methods have been developed to solve this problem [11]. By directly solving the coefficient matrix derived from Maxwell's equations, the precision of the method of moment (MOM) in analyzing the RCS characteristics of objects with different materials has been verified [12]. However, due to the too large matrix, this method is inefficient in investigating the RCS value of objects sized much larger than the radar wavelength, such as the intake. In order to solve these problems, the MLFMM has been developed and is widely used. Vogel [13] used the MLFMM to investigate the RCS characteristics of various fighters, and proved that the RCS characteristics of intake could be greatly affected by the compressor blades.

In order to suppress the radar echo intensity of intake, two methods have been proven to be effective. The first one uses the S-duct diffuser [14], coating the wall with low-scattering material [15]. A study on the aerodynamic and RCS characteristics of the double S-duct caret intake has proven that this method can be effective, but it could also lead to multiple boundary layer separations [16]. These separations could cause deterioration of outlet distortion [17]. Model parameters which could improve the stealth performance generally cause the loss of aerodynamic performance. Using the boundary layer bleed system can effectively suppress separation in the S-duct intake, but it could also lead to deterioration in the stealth performance [18]. Therefore, comprehensive analysis of the aerodynamic and stealth performance is necessary both for the design of S-duct intake [19] and for evaluating the effects of additional structures. Another method utilizes additional structures, such as the baffle board studied in this article, to increase the consumption of radar waves. Based on theoretical analysis of the supersonic intake, the baffle board could inevitably interfere with the high-speed airflow, resulting in the loss of aerodynamic performance. In addition, the RCS characteristics of intake may change once the board is exposed to the direct radiation of radar.

Hence, the objective of the present study is to optimize the configuration of the baffle board to effectively improve the stealth performance of intake while simultaneously reducing the associated loss of aerodynamic performance. In order to achieve this objective, the aerodynamic and stealth performances of double S-duct caret intakes with different baffle boards were investigated numerically, and the effects of baffle boards with different parameters were proposed in this study.

2. Computational Methodology

By employing applicable methods, the RCS and aerodynamic characteristics of the caret intake were analyzed initially. To suppress the radar echo intensity of intake, four curved baffle boards with the same area were installed at different locations of the S-duct diffuser. In order to further improve the stealth performance, four corrugated baffle boards were designed to replace the curved board with vertical orientation in the front diffuser. By investigating the effects of the corrugated baffle boards with different configurations, the RCS and aerodynamic characteristics of the caret intake were optimized.

2.1. Method Verification

To test for precision, the SST $k-\omega$ model was used to simulate the flow field of a mixed-compression intake, as shown in Figure 1 [20]. To ensure that all y^+ values were less than 1, a structured mesh with the first layer height of 0.0001 mm was used for the calculation. The surfaces of the intake model were set as the adiabatic standard no-slip wall. Using the commercial software Ansys Fluent 2020 R1 [21], the Reynolds-Averaged Navier-Stokes (RANS) equations were solved using the steady density-based formulation. The results of the experiment and calculation of the compression wall are presented in Figure 1b, with the ratio of static pressure to total pressure shown on the Y-axis. The results for the lip wall are presented in Figure 1c. It can be concluded that the SST model provides sufficient precision in calculating this type of supersonic intake flow field. Therefore, this

turbulence model was selected to numerically simulate the flow field of the S-duct caret intake.

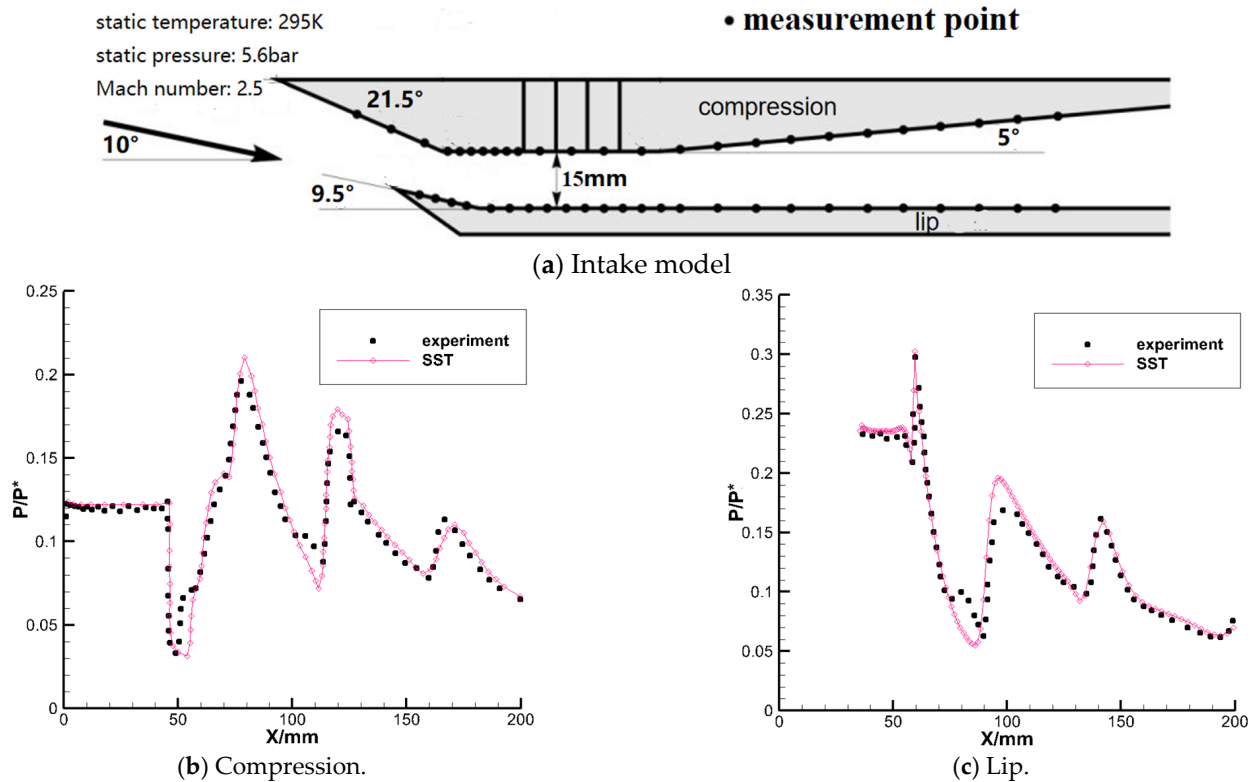


Figure 1. Verification for CFD method.

The RCS of an object can be defined by the projected area of an equivalent reflector with uniform radiation in all directions, which has the same echo power as the object in the unit solid angle of the receiving direction. In the vacuum environment, the RCS value can be solved for using Equation (1).

$$RCS = \lim_{R \rightarrow \infty} 4\pi R^2 \frac{S_s}{S_i} \tag{1}$$

S_s and S_i are the power densities of the scattered wave and the incident wave, respectively, and R is the distance between the object and the receiving system. The unit of RCS is m^2 , but the unit commonly used in practical application is dBsm. The conversion between the values with the two units can be defined as Equation (2).

$$RCS_{dBsm} = 10\lg(RCS_{m^2}) \tag{2}$$

Because the radar waves could be reflected several times inside a S-duct intake, which has a complex cavity structure, using the traditional cylinder or a dihedral angle to verify the accuracy of a CEM could be inaccurate for this phenomenon. Figure 2a depicts a complex cylindrical cavity [22] used to test the accuracies of four different methods. The model parameters are shown in Table 1. In addition to the two numerical solutions mentioned above, the physics optics (PO) method and the ray launching-geometrical optics (RL-GO) method are both approximate solutions. With the radar wave defined as a 5 GHz plane wave, the mesh for calculation was an unstructured mesh with the maximum size of 0.75 mm. Using the commercial software Altair Feko 2020.0.0 [23], the RCS values of this cylindrical cavity were calculated with the above four methods. Figure 2b,c present the results under the vertical polarization condition and the horizontal polarization condition, respectively. It could be concluded that the MOM and MLFMM

are more suitable for calculating the cavity RCS value compared to the other two methods. Due to the inefficiency of the MOM in solving large objects, the MLFMM was chosen as the most suitable method to investigate the intake stealth performance.

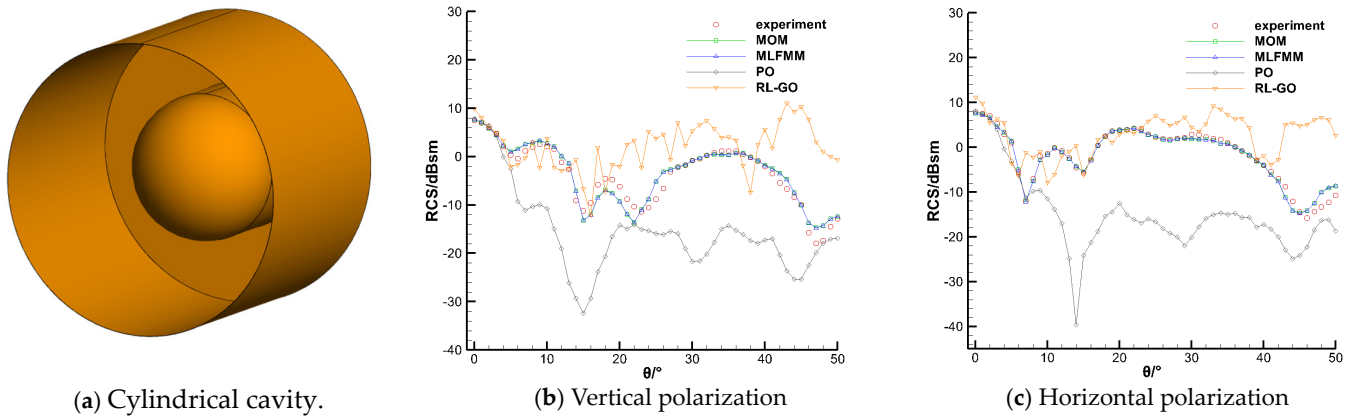


Figure 2. Model and RCS results at two polarization conditions.

Table 1. Model parameters of the complex cylindrical cavity.

Cavity		Cylinder	
Diameter/m	Length/m	Diameter/m	Length/m
0.286	0.3	0.16	0.16

2.2. Intake Models and Calculation Conditions

In order to study the effects of different S-duct diffusers, two intake models were designed: a single S-duct caret intake, named Model A, and a double S-duct caret intake, named Model B, as shown in Figure 3a. Both intakes had an ideal capture flow rate of 80.55 kg/s at an altitude of 15 km, and a Mach number of 2. The configuration parameters of the two intakes were the same, except for the Z-coordinate of each diffuser section center. The inlet shape of the intake was a parallelogram to match the aircraft’s RCS characteristic. As shown in Figure 3b, the section shape of the S-duct diffuser changed from a parallelogram to an equal-height rectangle in the front diffuser, and then to a circle in the rear diffuser, with the area increasing from 0.502 m² to 0.636 m². Figure 3c presents the center coordinate of each double S-duct diffuser section, with the area shown in Figure 3d.

To further reduce the radar echo intensity, various baffle boards were installed in the diffuser, and the performances of these intakes were numerically investigated. Initially, four curved baffle boards with nearly the same surface area were installed at different locations in the diffuser, as shown in Figure 4a. The detailed dimensions of these boards are provided in Figure 4b. After determining the optimal installation location, seven corrugated baffle boards were designed and installed at locations similar to model C-2 to optimize the RCS characteristics of the intake. The design approach for the corrugated baffle board is depicted in Figure 4c. Taking a cross-section as an example, the coordinate system was established with the center point of the lower wall set as the origin. The mapping curve of the corrugated baffle board in this section could be expressed by a functional relationship. The functional parameters of each board are shown in the table, and the models of these boards are depicted in Figure 4d. The optimal corrugation number can be determined by comparing the performances of the intakes with the first four boards. Subsequently, the optimal corrugation shape can be determined by comparing the performances of the intakes with the remaining boards.

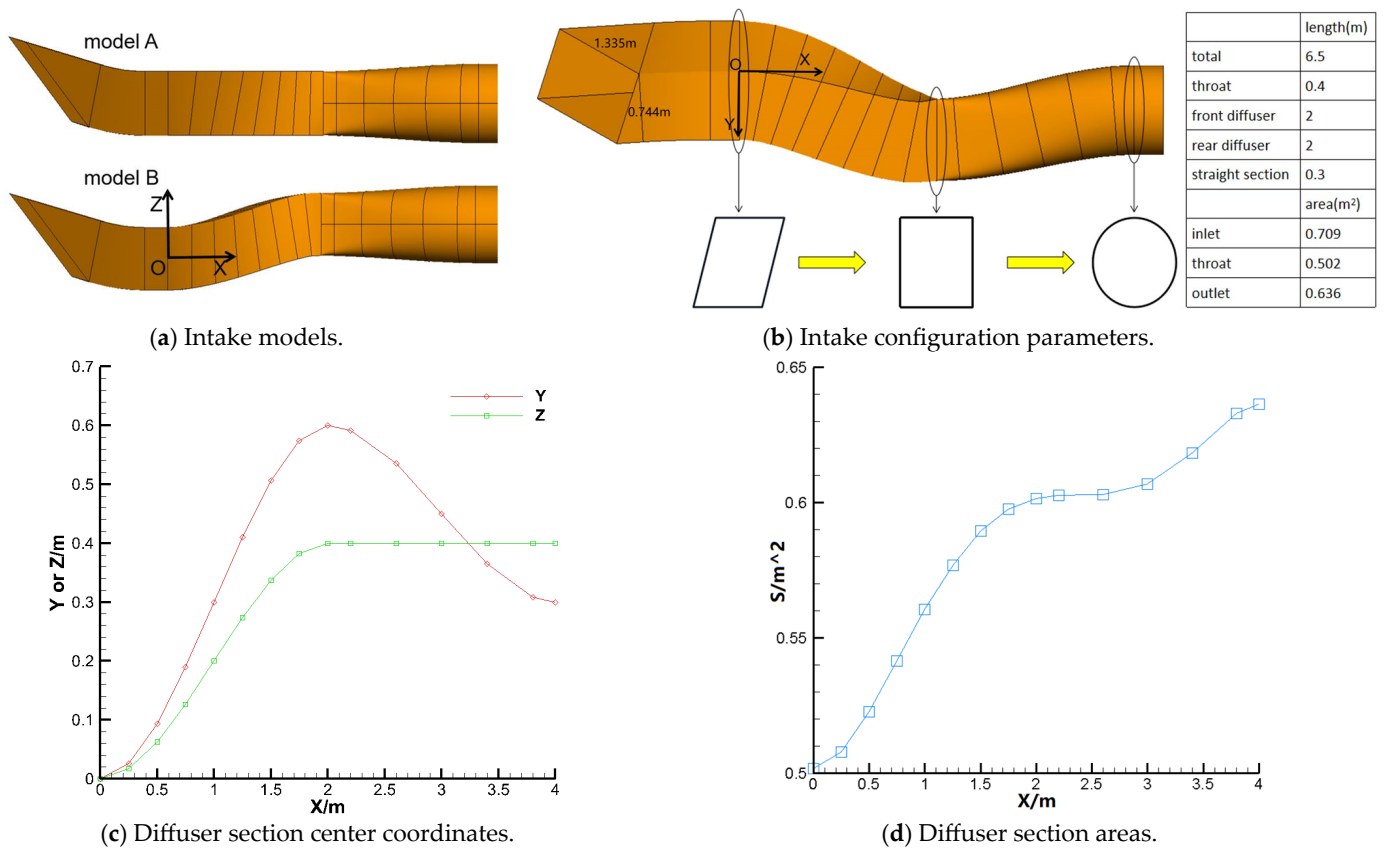


Figure 3. Models and parameters of two S-duct intakes.

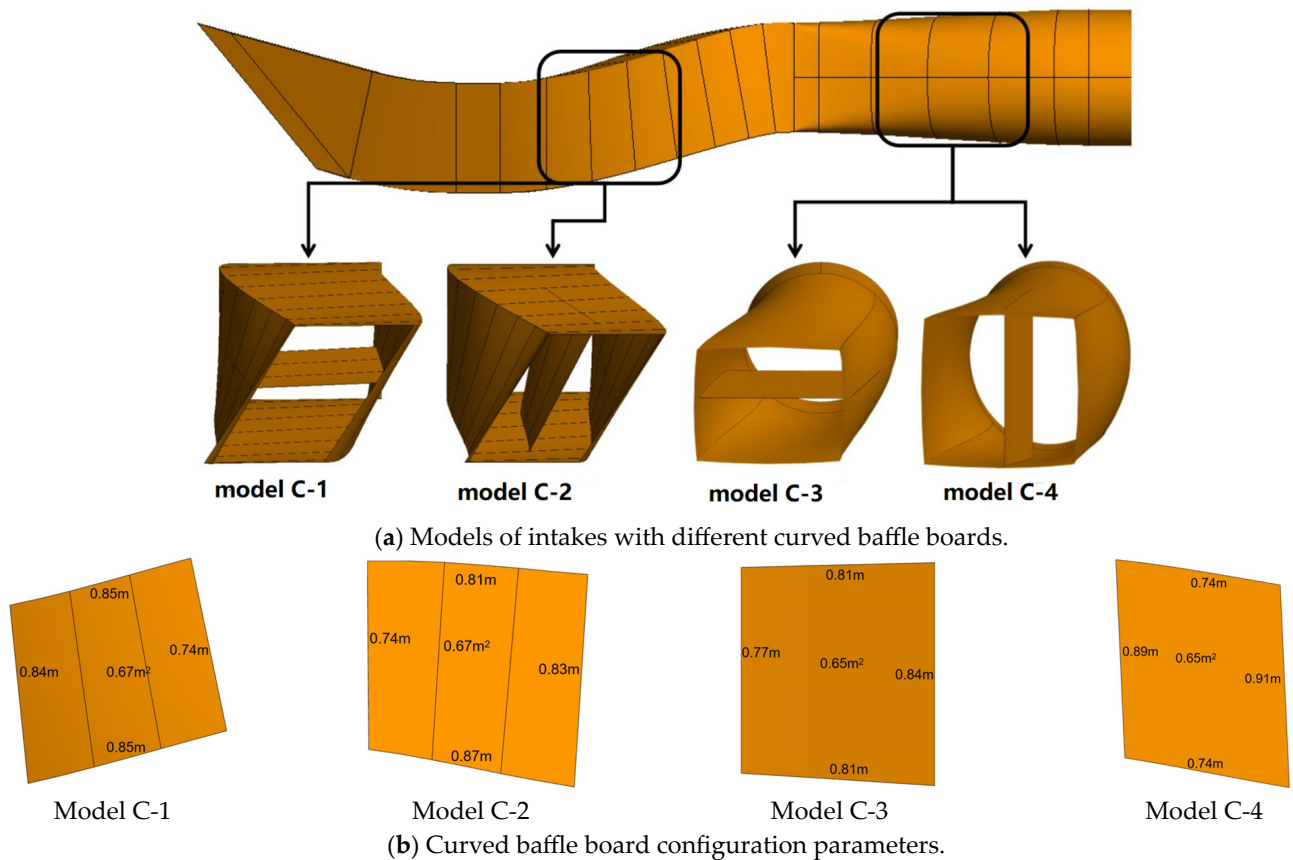
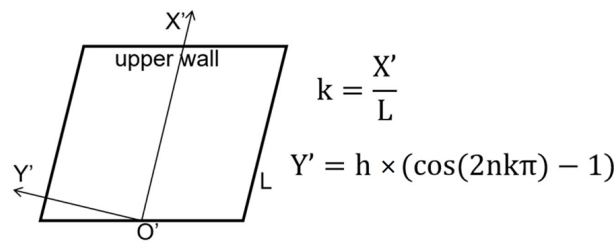
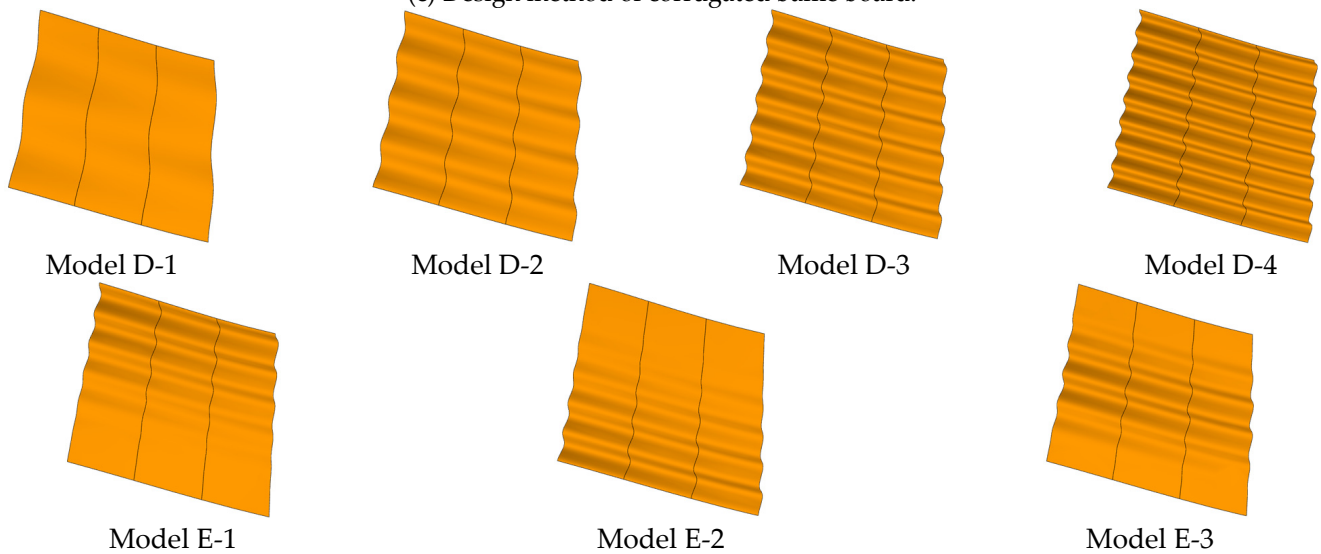


Figure 4. Cont.



	model D-				model E-		
	1	2	3	4	1	2	3
h/mm	20	20	20	20	$10 \times (1 - \cos(k\pi))$	$10 \times (1 - \cos(2k\pi))$	$10 \times (1 + \cos(k\pi))$
n	2	4	6	8	6	6	6

(c) Design method of corrugated baffle board.



(d) Models of different corrugated baffle boards.

Figure 4. Models and parameters of double S-duct caret intakes with different baffle boards.

Low-scattering material is generally coated on the surfaces of intakes to reduce the RCS. To minimize the errors caused by the direct radiation of radar waves on the outer wall, each intake was enclosed in a uniform cavity during the RCS calculation, as shown in Figure 5a. Additionally, the surfaces of each calculation model were coated by radar stealth material with relative magnetic permeability $\mu = 1.29 - 0.57j$ and relative dielectric constant $\epsilon_r = 9.72 - 1.08j$, except for the ideal electrical conductor outlet. The radar wave used was the 3 GHz plane wave, and the frequency of the incident radar wave was the median of the S band, which is often used as the radar band of early warning aircraft. As illustrated in Figure 5b, the $X''O''Y''$ plane was defined as the horizontal plane, and the interval between the two incident angles was 1° , parallel to the horizontal plane. Point O'' represented the inlet apex of the intake. The calculation conditions of the flow field are presented in Figure 5c, where the direction of the incoming flow was parallel to the X-axis. The flow coefficient, the TPR coefficient, and the DC60 were used to measure the aerodynamic performance of the intake. The flow coefficient was the ratio of the outlet flow to the inlet design flow, and can be calculated using Equation (3).

$$\varphi = \frac{m_{out}}{m_{in,design}} \tag{3}$$

The DC60 was used to measure the total pressure distortion at the outlet [24]. The greater the DC60 value, the more uneven the total pressure distribution of the flow along the circumference. The DC60 value can be calculated using Equation (4).

$$DC60 = \frac{\overline{P^*} - \overline{P_{min}^*(60)}}{\overline{q}} \tag{4}$$

where $\overline{P_{min}^*(60)}$ is the minimum average total pressure of the sector with an angle of 60° at the outlet, and \overline{q} is the average dynamic pressure at the outlet. The TPR coefficient can be calculated using Equation (5).

$$\sigma = \frac{\overline{P_{out}^*}}{\overline{P_{far}^*}} \tag{5}$$

$\overline{P_{out}^*}$ is the average total pressure at the outlet and $\overline{P_{far}^*}$ is the average total pressure of the incoming flow.

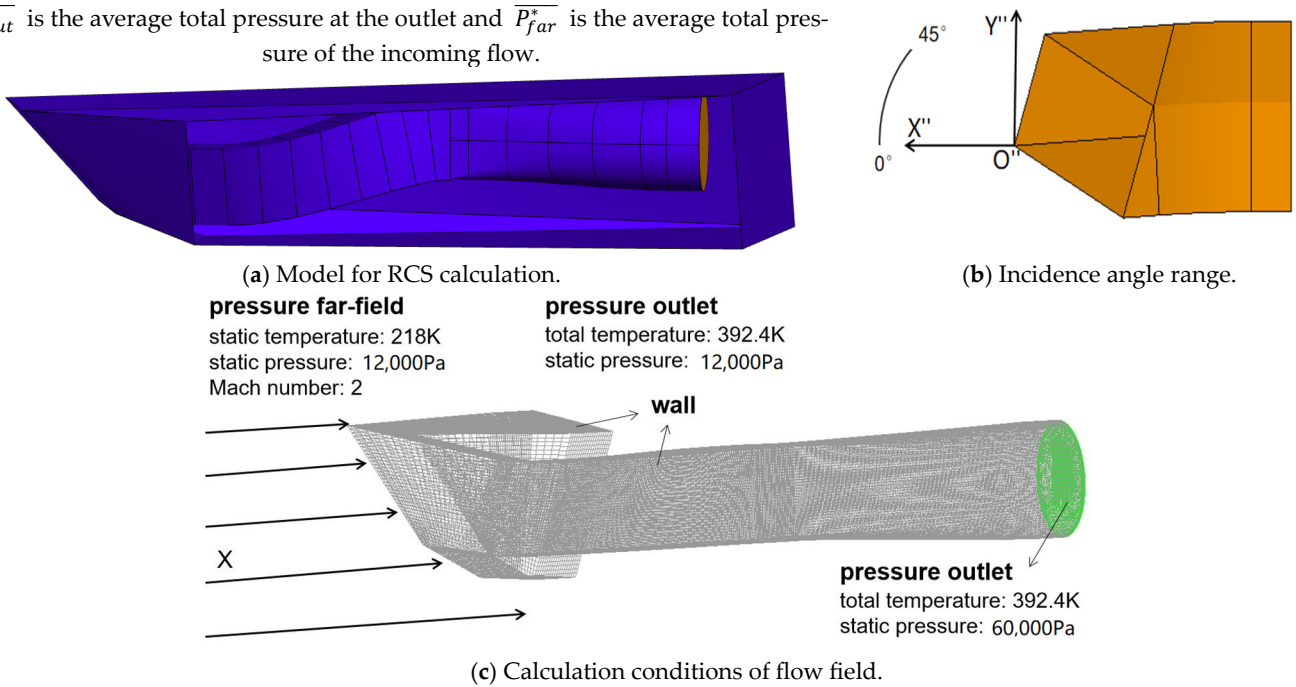


Figure 5. Calculation conditions of RCS and flow field.

2.3. Study of Mesh Dependency

To ensure calculation accuracy and maximize efficiency, mesh independence was studied under the aforementioned conditions. For the vertical polarization condition, the RCS value at an angle of 0° was investigated using the MLFMM with a sparse approximate inverse preconditioner. The convergence criterion was set such that the residual was less than 0.01. To maintain y^+ values between 0 and 10, a structured mesh with a first layer height of 0.02 mm was used for the calculation. During the simulation of the flow field, the convergence criterion for the flow rate sum of the two outlets and an inlet was set to be less than 0.01 kg/s, while the residuals of k and x -velocity continuity were both less than 0.001. Figure 6 shows the inner wall y^+ value and the calculation results. The numbers of different mesh types and the corresponding calculation results are presented in Table 2. During the flow field calculation, when the total mesh number was less than 2.4 million, both the outlet total pressure distribution and the two parameters changed significantly with an increase in the mesh number. A similar phenomenon was observed in the RCS calculation, with a critical mesh number of 1.02 million. Therefore, the flow field and RCS values were calculated using mesh types with 2.4 million and 1.02 million elements, respectively.

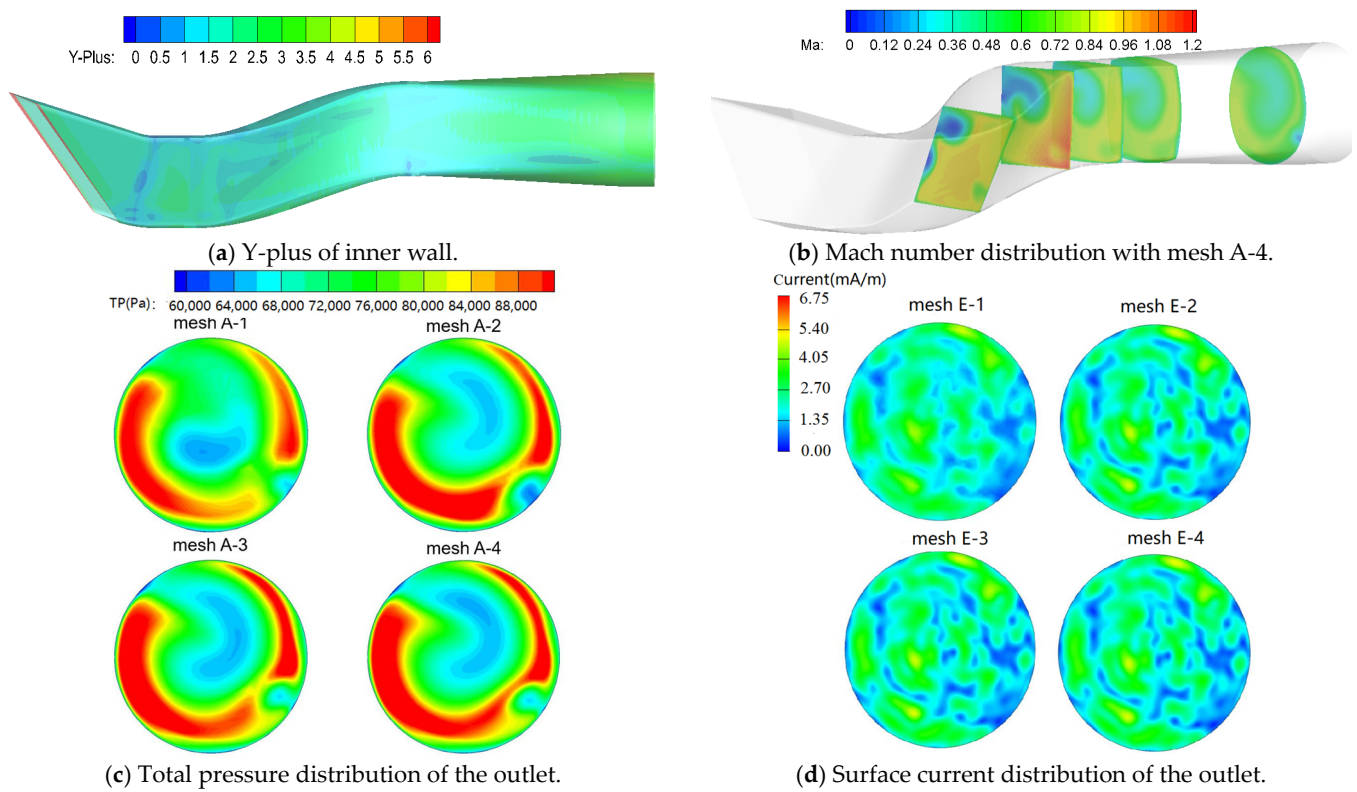


Figure 6. Y-plus of inner wall and parameter distributions of the outlet.

Table 2. Mesh type and performance parameters.

Mesh Type	Aerodynamic Performance				Electromagnetic Performance			
	Mesh Number (million)		Flow (kg/s)	Average Total Pressure (Pa)	Mesh Type	Mesh Size	Mesh Number (million)	RCS (dBsm)
	Inner	Whole						
mesh A-1	0.54	0.83	80.133	76,811.5	mesh E-1	$\lambda/4$	0.26	3.95
mesh A-2	1.02	1.33	80.138	77,088.2	mesh E-2	$\lambda/6$	0.71	3.37
mesh A-3	1.98	2.41	80.145	77,203.9	mesh E-3	$\lambda/8$	1.02	3.13
mesh A-4	3.95	4.69	80.146	77,228.8	mesh E-4	$\lambda/10$	1.59	3.11

3. Results and Analysis

3.1. Characteristic Analysis of S-Duct Caret Intake

Figure 7 shows the RCS values of the two intakes at different radar incidence angles, and the stealth performance parameters are presented in Table 3. In addition to the three common statistical values of RCS, a new term named low scattering angle (LSA) is proposed, which corresponds to a RCS value of the intake that is less than 0 dBsm. Therefore, the higher the value of the LSA, the more conditions the intake can be safely applied to. According to Figure 7a, under the horizontal polarization condition, the RCS values of each intake were all below 0 dBsm with radar incidence angles over 20°, indicating that both intakes had excellent lateral stealth capability. However, the RCS values of Model A were almost all significantly greater than 0 dBsm with incidence angles less than 10°, resulting in the maximum value and the average value being as high as 12.71 dBsm and 2.49 dBsm, respectively. Therefore, the traditional S-duct intake had an obvious fatal defect in stealth performance. In contrast, the RCS values of Model B were generally smaller than those of Model A at most angles, with the average value reduced to −0.87 dBsm and the LSA number increasing to 36. A similar conclusion could also be proposed for the other polarization condition, except that the RCS values of Model B were higher than those of Model A, with angles between 13° and 23°. Therefore, it can be concluded that the double

S-duct diffuser could significantly improve the stealth performance of the caret intake, but the RCS values at some angles still need to be reduced.

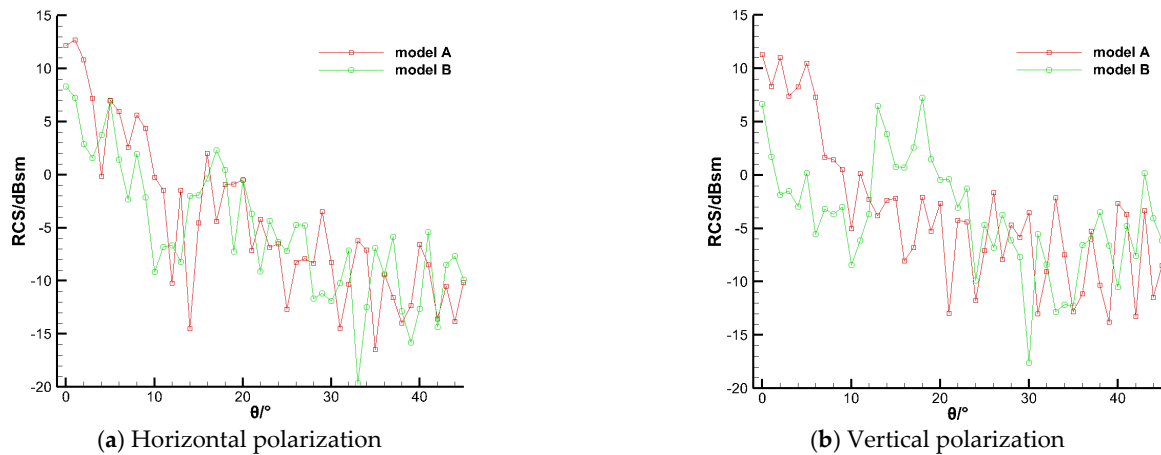


Figure 7. RCS values of two S-duct intakes.

Table 3. Stealth performance parameters of two intakes.

Model	Horizontal Polarization				Vertical Polarization			
	RCS (dBsm)			Number of LSA	RCS (dBsm)			Number of LSA
	Maximum	Average	Minimum		Maximum	Average	Minimum	
A	12.71	2.49	-16.47	35	11.29	2.26	-13.78	34
B	8.3	-0.87	-19.64	36	7.28	-0.93	-17.56	35

The flow field calculation results of the two intakes are shown in Figure 8, with the aerodynamic parameters calculated in Table 4. According to Figure 8c, for each intake, an oblique shock wave was formed at the inlet and a positive shock wave was formed at the throat, indicating that both intakes were at the critical state with an outlet pressure of 60,000 Pa. The Mach number distribution in the diffuser revealed a boundary layer separation phenomenon in both S-duct intakes.

Table 4. Aerodynamic characteristics of two intakes.

Model	Flow Coefficient	TPR Coefficient	Distortion Index DC60
A	0.9943	0.8289	0.5381
B	0.9942	0.8211	0.1847

Taking Model A as an example, two obvious separations occurred near the upper and lower walls on one side of the front diffuser, resulting in two corresponding low-pressure zones at the outlet. As the diffuser wall compressed, the airflow near the other side accelerated to supersonic speed, forming a local shock wave at the S-bend. Due to the interaction between this local shock wave and the boundary layer, a strong separation also occurred in the rear diffuser, leading to an obvious low-pressure zone at the outlet. Therefore, the DC60 values of Model A exceeded 0.53, indicating that the traditional S-duct intake also had a significant aerodynamic performance defect. In contrast, there was only one separation in the front diffuser of Model B, and the low-speed airflow resulting from this separation could be mixed with the high-speed flow in the rear diffuser, leading to the corresponding low-pressure zone being mainly distributed around the outlet center. Additionally, the separation in the rear diffuser was slightly suppressed. Therefore, compared with the traditional S-duct intake, the DC60 value of the double S-duct intake decreased by 0.35, with the TPR coefficient only decreasing by 0.008.

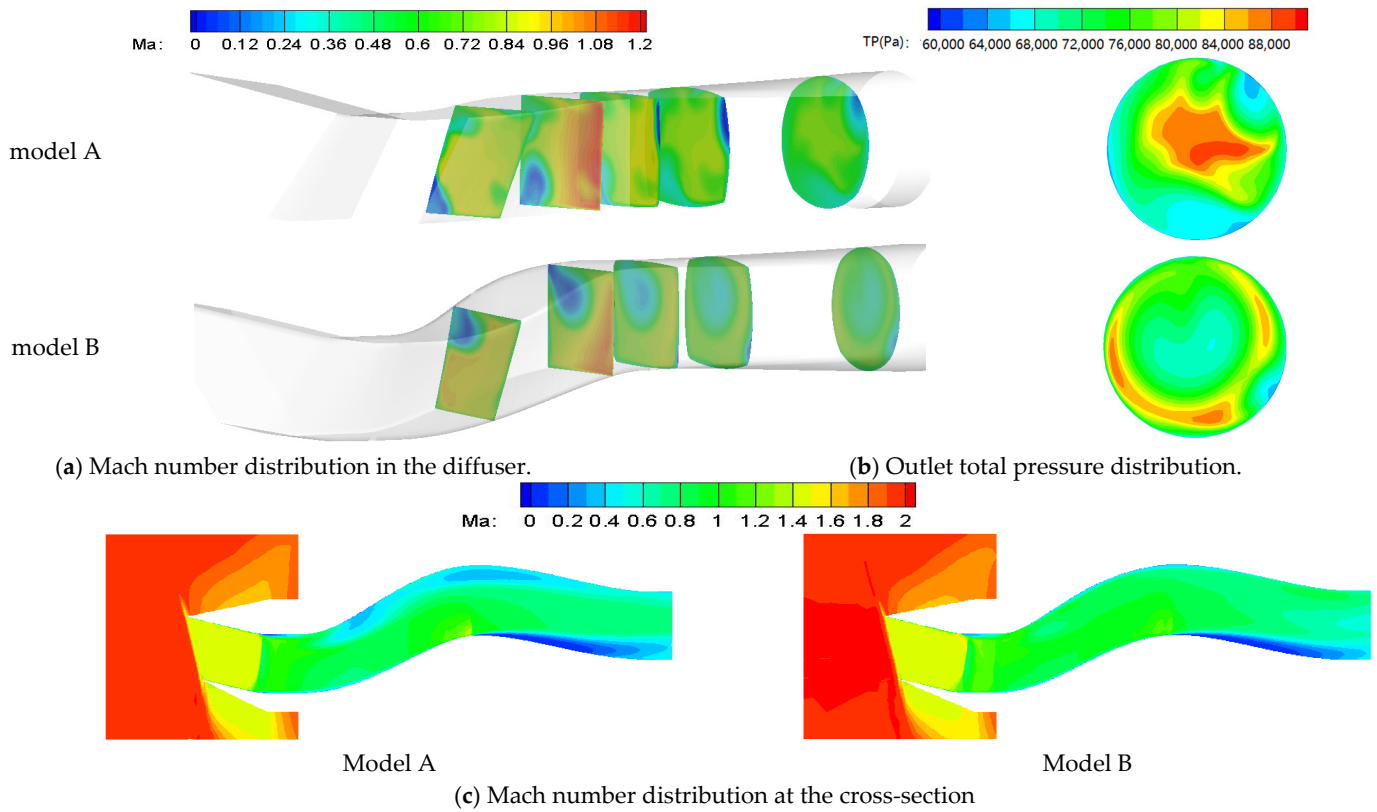


Figure 8. Flow field calculation results of two intakes.

3.2. Effect of Curved Baffle Board Locations

Figure 9 presents the RCS values of the four double S-duct intakes with curved baffle boards installed at different locations. The stealth performance and aerodynamic performance parameters are displayed in Table 5. According to Figure 9, the RCS values of the four intakes varied similarly with the incidence angle, indicating that the baffle board played a relatively minor role in the RCS characteristics of the intake. However, the RCS values of the four intakes differed significantly at the same incidence angle, especially at angles like 9° and 18° with the vertical polarization condition.

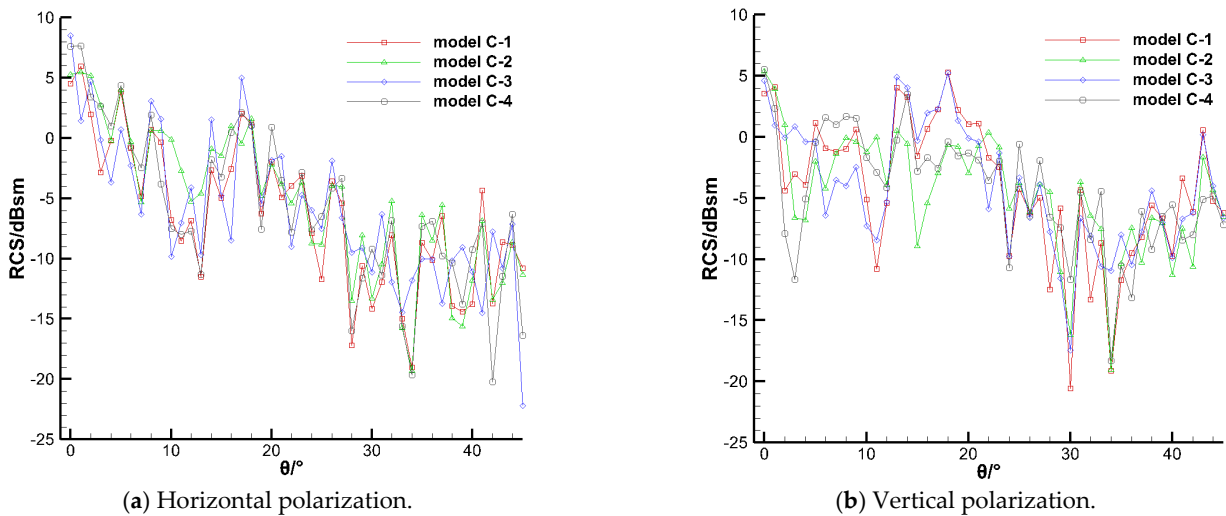


Figure 9. RCS values of intakes with different curved baffle boards.

Table 5. RCS and aerodynamic characteristics of intakes with different curved baffle boards.

Polarization	RCS/(dBsm)	Model C-1	Model C-2	Model C-3	Model C-4
horizontal	average	−2.23	−1.11	−1.77	−1.17
	maximum	7.95	7.49	8.51	7.66
	value of LSA	39	37	37	36
vertical	average	−1.44	−2.10	−1.43	−1.78
	maximum	5.31	5.38	5.25	5.54
	value of LSA	34	39	34	38
	flow coefficient	0.9943	0.9950	0.9860	0.9743
	TPR coefficient	0.8154	0.8147	0.8189	0.8126
	distortion index DC60	0.3088	0.2452	0.3472	0.2723

Table 5 shows that compared with Model B, the RCS values of the four intakes were generally reduced, and the LSA numbers were generally increased, demonstrating that the baffle board coated with low-scattering material could be highly effective in improving the stealth performance of the intake. Additionally, the average RCS values of Model C-1 and Model C-3 under at the horizontal polarization condition were both below -1.7 dBsm, while the values under the other condition both exceeded -1.5 dBsm, indicating that the horizontal board was more effective under horizontal polarization. Similar conclusions can be drawn from the values of the other two models. Under the horizontal polarization condition, the average and maximum RCS values of Model C-3 were both greater than those of Model C-1. However, under the other condition, there was little difference between the parameters of the two intakes. Similarly, under the vertical polarization condition, the stealth performance of Model C-2 was obviously better than that of Model C-4, but there was no difference under the other condition. Therefore, it could be concluded that the baffle board in the front diffuser was more effective in reducing the RCS of the double S-duct intake than the board in the rear diffuser. Notably, the LSA number of Model C-1 still needs to be increased under the vertical polarization condition, and the RCS values of Model C-2 at some angles also need to be reduced under the horizontal polarization condition.

In terms of aerodynamic performance, the flow field results of the four intakes are shown in Figure 10. According to Figure 10b, a significant difference occurred between the flow zones on the two sides of each baffle board, inevitably leading to changes in the outlet total pressure distribution and enhancing the flow mixing effect.

Therefore, compared with the values of Model B, the DC60 values of the four intakes all increased above 0.24, and the TPR coefficients were all reduced. There was an obvious low-speed zone in the rear diffuser of Model C-3 and Model C-4, respectively, indicating that the baffle board in the rear diffuser could aggravate boundary layer separation. Due to the decrease in the actual flow area caused by the low-speed zone, the flow coefficients of the two models both reduced below 0.99. However, the baffle boards of the other two models had no effect on the flow coefficients. Additionally, due to the short distance between the outlet and the baffle board in the rear diffuser, the downstream flow mixing effect had little influence on the suppression of the low-speed zone and the discontinuity between the flow at the two sides of the board. Therefore, with the same orientation of the baffle boards, the DC60 values of Model C-3 and Model C-4 were respectively higher than those of Model C-1 and Model C-2. It could be concluded that the baffle board in the front diffuser has a lesser adverse effect on the aerodynamic performance of the double S-duct intake, compared with the board in the rear diffuser.

Additionally, because the flow distribution along the Y-axis direction was more uneven than along the Z-axis direction in the double S-duct intake, the DC60 value of Model C-2 was 0.06 lower than that of Model C-1.

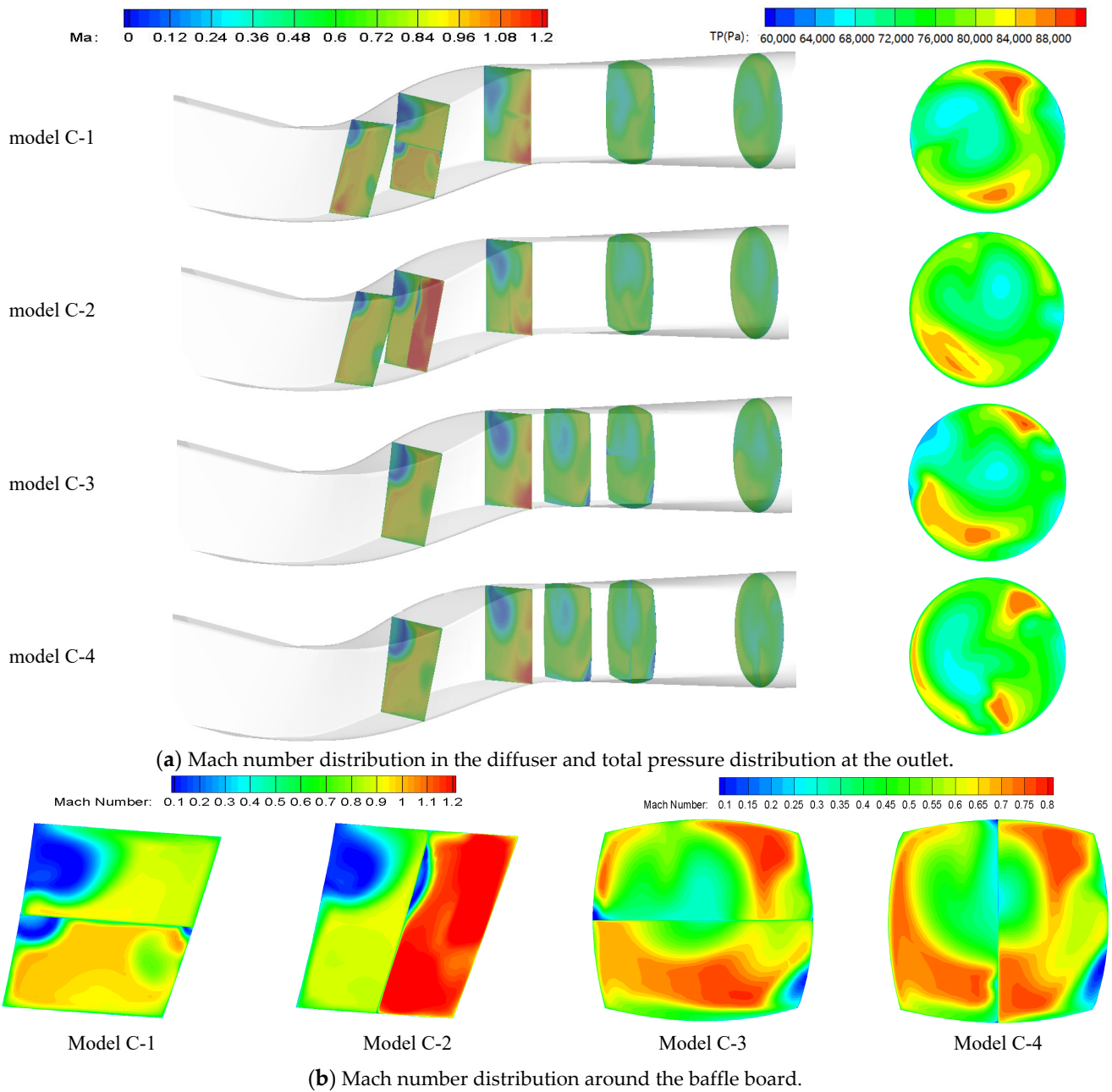


Figure 10. Flow field results of intakes with different curved baffle boards.

3.3. Effect of Corrugated Baffle Board

In order to further improve the radar stealth performance of the double S-duct intake under the horizontal polarization condition, four corrugated baffle boards with different corrugation numbers were designed to replace the curved board. The location and orientation of the four corrugated boards were all the same as those of the curved board in Model C-2. Figure 11 shows the RCS values of the four intakes with the different corrugated boards. The stealth performance and aerodynamic performance parameters are calculated in Table 6. According to Figure 11, under both polarization conditions, the RCS values of the four intakes were significantly different at the same incidence angle when the angle is less than 20°. Precisely in this range of the radar incidence angle, improving the stealth performance of the double S-duct intake is extremely important. Therefore, it is necessary to study the effect of the corrugated baffle board shape on both performances of the intake.

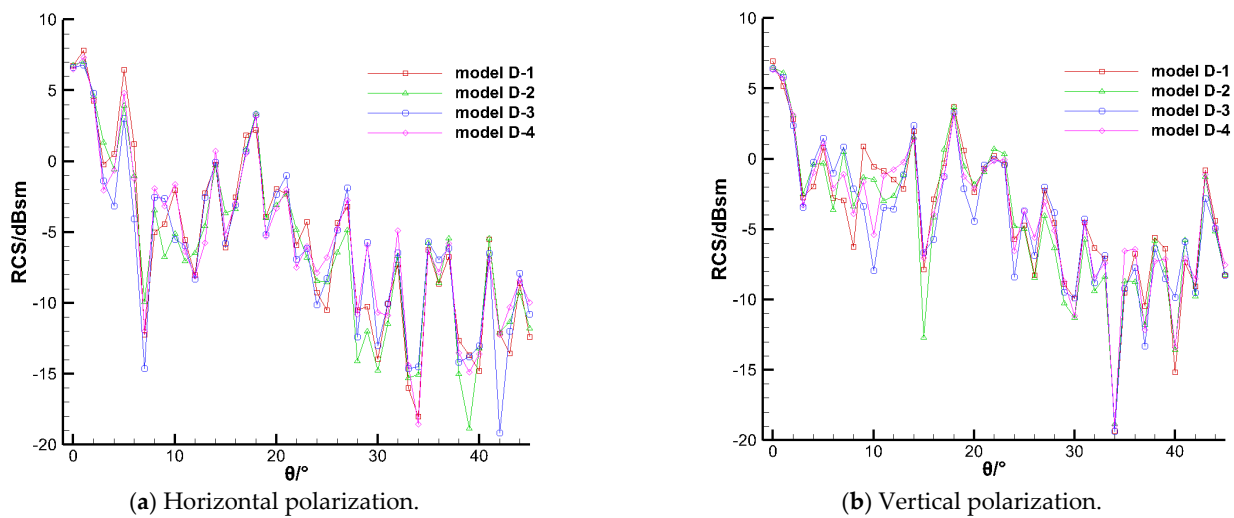


Figure 11. RCS values of intakes with different corrugated baffle boards.

Table 6. RCS and aerodynamic characteristics of intakes with different corrugated baffle boards.

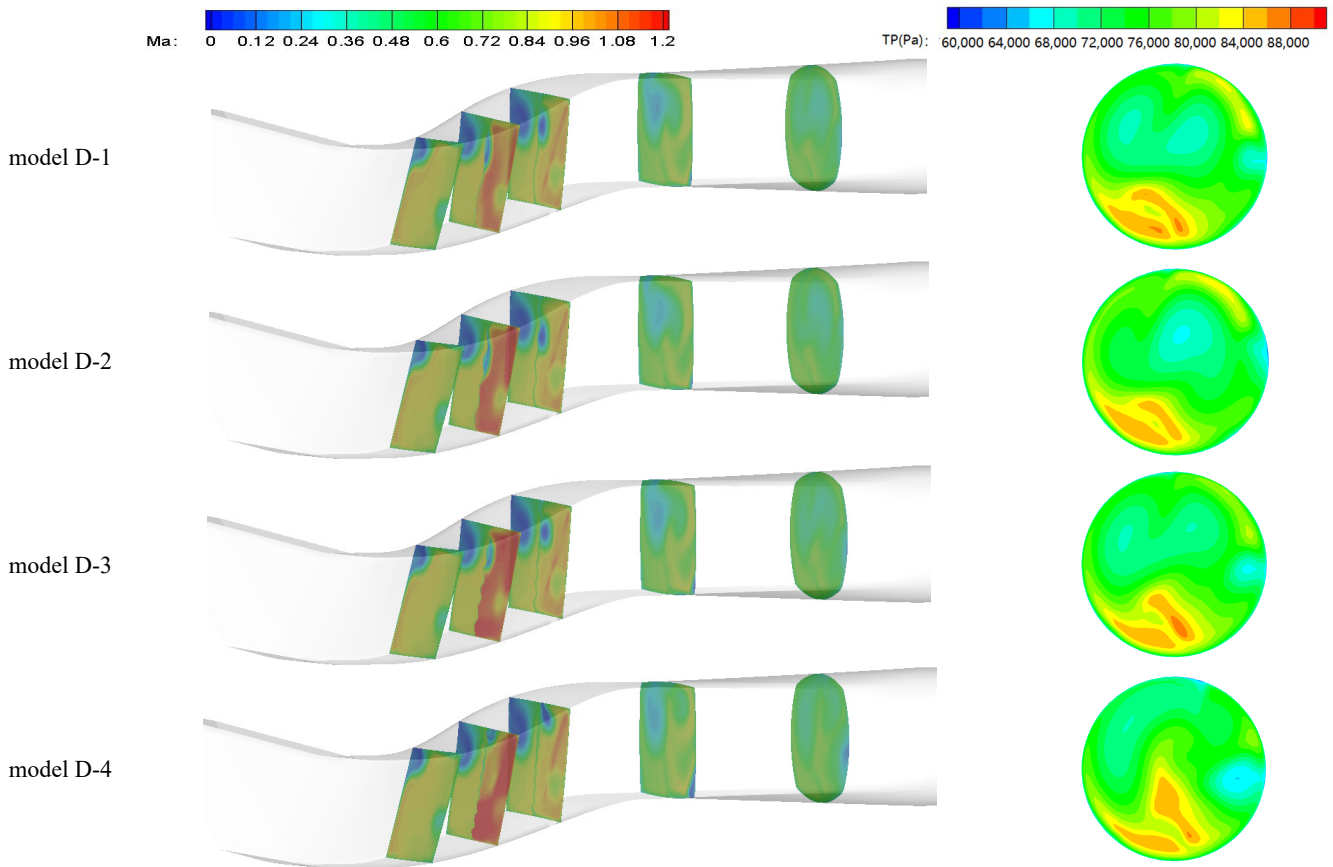
Polarization	RCS/(dBsm)	Model D-1	Model D-2	Model D-3	Model D-4
horizontal	average	−1.47	−1.71	−2.01	−1.82
	maximum	7.82	7.04	6.77	7.34
	number of LSA	38	39	40	39
vertical	average	−1.38	−1.46	−1.56	−1.61
	maximum	6.95	6.49	6.41	6.33
	number of LSA	37	37	39	40
	flow coefficient	0.9952	0.9949	0.9949	0.9946
	TPR coefficient	0.8144	0.8131	0.8128	0.8141
	distortion index DC60	0.2694	0.2498	0.2582	0.2610

According to the data in Table 6, under the horizontal polarization condition, the average RCS values of the four intakes with the corrugated boards reduced to below -1.45 dBsm, and the LSA values also increased to more than 38, compared with Model C-2. Except for Model D-1, the maximum RCS values of the other three models were all reduced to about 7 dBsm. However, under the vertical polarization condition, the stealth performance parameters of the four models had generally deteriorated. Therefore, it could be concluded that the corrugated baffle board can effectively reduce the gap between the intake stealth performances under the two polarization conditions, which was caused by the curved board with vertical orientation.

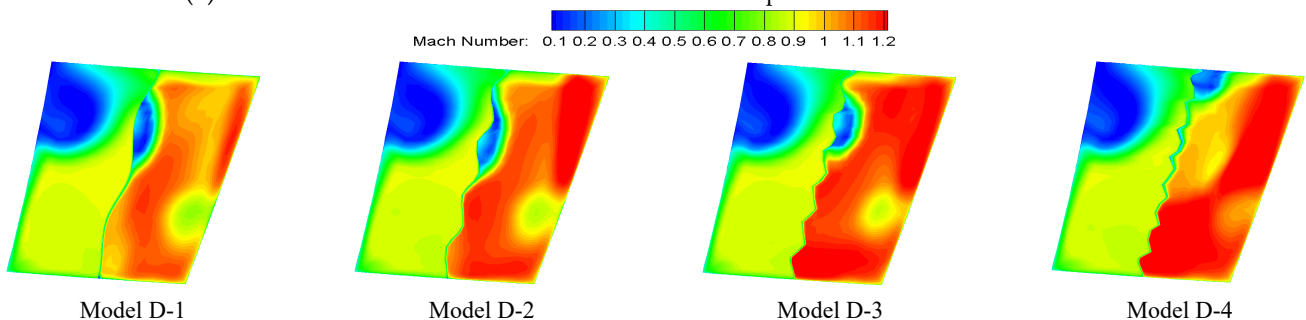
Under the horizontal polarization condition, with the corrugation number of the baffle board increased, the maximum and average RCS values of the intake both decreased first and then increased, while the LSA value increased first and then decreased. Among these, the stealth performance of Model D-3 with the corrugation number of 6 was the best. Under the vertical polarization condition, the stealth performance of the intake was improved with increased corrugation number.

In terms of the aerodynamic performance, the flow field results of the four intakes are shown in Figure 12. When the corrugation number of the baffle board was less than seven, there was no obvious difference among the Mach number distributions in the diffusers of the three models and the Model C-2, except for the shape of the low-speed zone on the side of the supersonic flow. Similarly, the outlet pressure distributions of the three intakes were only slightly different in the shape of the high-pressure zone, compared with the results of the model C-2. Therefore, according to the data in Table 6, although the flow coefficients were still around 0.9950, the TPR coefficients of the three intakes were all reduced and the DC60 values all increased, compared with the parameters of the Model C-2.

In addition, the TPR coefficient of the intake decreased with an increase in the corrugation number. However, according to the results of the Model D-4, with a corrugation number of eight, the location and the shape of the low-speed zone on the side of the supersonic flow in the front diffuser both changed, with boundary layer separation occurring in the rear diffuser. Therefore, the flow coefficient of the model D-4 was only 0.9946. In addition, if the corrugation number continued to increase, the intake outlet flow rate would further decrease and fluctuate regularly during the numerical simulation, which indicates that a reflux phenomenon occurred in the diffuser due to the intensification of the boundary layer separation.



(a) Mach number distribution in the diffuser and total pressure distribution at the outlet.



(b) Mach number distribution around the baffle board.

Figure 12. Flow field results of intakes with different corrugated baffle boards.

Therefore, with the parameter h in the ripple function set as two, the optimal corrugation number for the corrugated baffle board is six. With this corrugated board, the double S-duct intake could have excellent stealth performance under each polarization condition and applicative aerodynamic performance under the design condition.

3.4. Corrugation Shape Optimization of Baffle Board

To investigate the influence of corrugation shape on the effect of the corrugated baffle board, three corrugated boards with the same corrugation numbers but different shapes were designed and installed at the same positions on the front diffuser as above. The large-curvature zones of the corrugated boards in the three models were designed, respectively, near the upper wall, at the middle part of the board, and near the lower wall. Figure 13 shows the RCS values of the three intakes. The stealth performance and aerodynamic performance parameters are calculated in Table 7. Compared with the Model D-3, the stealth performances of the three intakes all deteriorated under the horizontal polarization condition and were all optimized under the other condition, which was consistent with the comparative conclusion regarding the effects of the curved board and corrugated board mentioned above.

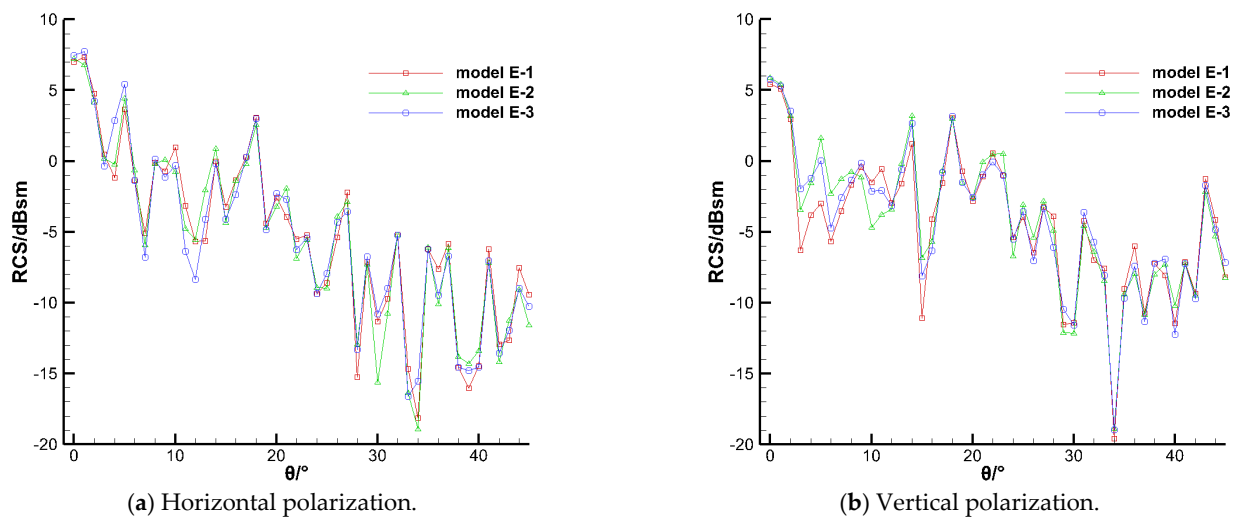


Figure 13. RCS values of intakes with shape-optimized baffle boards.

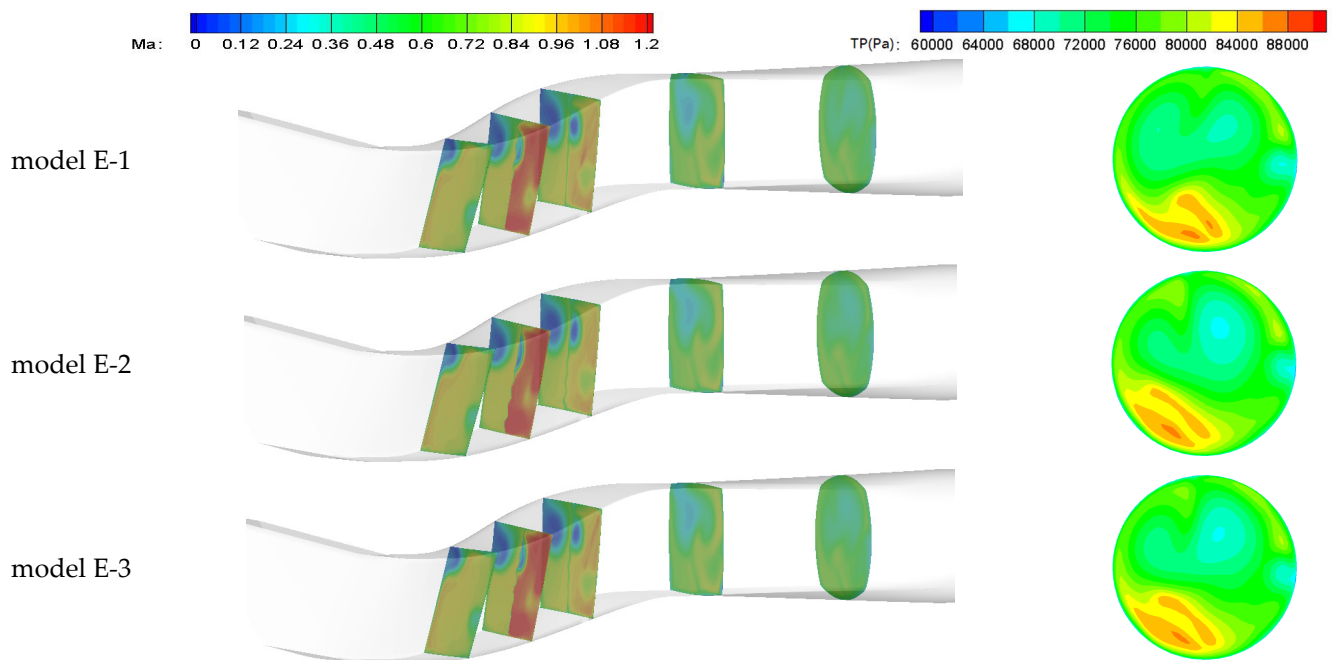
Table 7. RCS and aerodynamic characteristics of intakes with shape-optimized baffle boards.

Polarization	RCS/(dBsm)	Model E-1	Model E-2	Model E-3
horizontal	average	-1.46	-1.52	-1.18
	maximum	7.32	7.25	7.65
	number of LSA	38	38	38
vertical	average	-2.04	-1.75	-1.89
	maximum	5.44	5.88	5.77
	number of LSA	40	39	40
	flow coefficient	0.9950	0.9950	0.9950
	TPR coefficient	0.8128	0.8142	0.8139
	distortion index DC60	0.2596	0.2382	0.2405

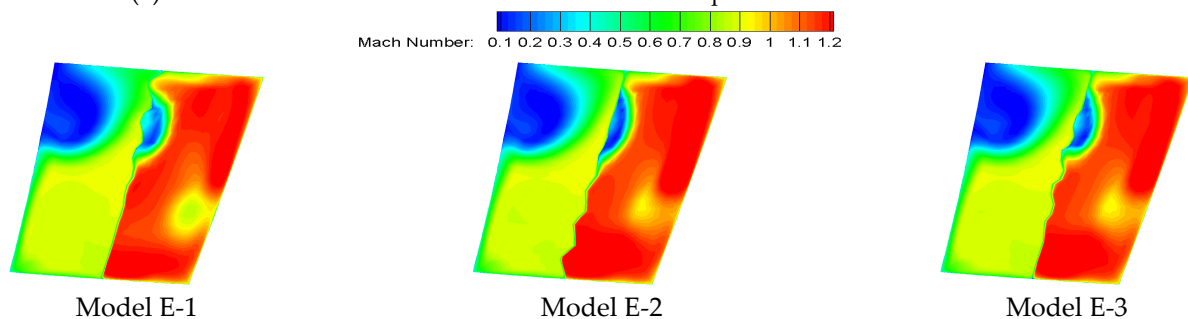
According to Figure 13a, under the horizontal polarization condition, there was almost no difference between the RCS values of the three intakes at the same incidence angle, except that the values of the Model E-3 were significantly greater than those of the other two models when the angle was less than 5° . Therefore, with the same LSA number, the maximum and average RCS values of the Model E-3 were both the largest, while the performance parameters of the other two models were generally similar. Additionally, the performance parameters of the Model E-3 were also generally similar to the Model C-2, in which the curved board was installed. It could be concluded that the curvature of the middle part had only a slight influence on the effect of the baffle board in improving the intake stealth performance under the horizontal polarization condition.

Under the vertical polarization condition, there were obvious differences among the RCS values of the three intakes at the same incidence angle when the angle was less than 15° , meaning that the corrugation shape had a significant influence on the effect of the corrugated baffle board. The closer the large-curvature zone of the corrugated board was to the upper wall, the smaller the maximum and average RCS of the model, and the better the intake stealth performance.

In terms of the aerodynamic performance, the flow field results of the four intakes are presented in Figure 14. By comparison, the flow field distribution and the aerodynamic performance parameters of the Model E-1 were generally the same as those of the Model D-3. Similarly, there was not much difference between the calculated results of the Model E-2 and the Model C-2. The aerodynamic performance of the Model E-3 was between those of the other two models. The reason for this phenomenon was that the boundary layer separation in the supersonic zone was aggravated as the curvature of the corrugated board near the upper wall increased. Therefore, it could be concluded that the closer the large-curvature zone of the corrugated board is to the upper wall, the worse the intake aerodynamic performance.



(a) Mach number distribution in the diffuser and total pressure distribution at the outlet.



(b) Mach number distribution around the baffle board.

Figure 14. Flow field results of intakes with shape-optimized baffle boards.

4. Conclusions

According to the results of the numerical investigation, the following conclusions can be obtained:

I. The double S-duct diffuser could effectively suppress the radar echo intensity of the caret intake under both polarization conditions, but there were several boundary layer separations in the diffuser. The curved baffle board could further improve the stealth performance of the intake, and the effect of the baffle board in the front diffuser was more obvious than that of the board in the rear diffuser with the same orientation. However, the board can aggravate the separation, which could increase the outlet distortion and even reduce the flow coefficient. By comparison, the vertical board in the front diffuser caused the least loss of aerodynamic performance, but the improvement in stealth performance under the horizontal polarization condition was obviously worse than that under the other condition.

II. By using the corrugated board instead of the curved board, the difference between the improvements in stealth performance under the two conditions was reduced. Until the corrugation number of the corrugated board reached eight, the aerodynamic performance of intake changed insignificantly with the corrugation number. The improvement in the stealth performance under the vertical polarization condition can be enhanced with an increase in the corrugation number. Under the other condition, the improvement in the stealth performance was the best when the corrugation number was six.

III. By partly changing the curvature of the corrugated baffle board, the RCS characteristics and the aerodynamic performance of the intake can be both optimized. The curvature of the middle part of board had only a slight influence on the improvement in the stealth performance under the horizontal polarization condition. The closer the large-curvature zone was to the upper wall of the intake, the better the stealth performance under the vertical polarization condition, but the worse the aerodynamic performance.

In conclusion, while the corrugated baffle board improved the stealth performance of the intake, it could also inevitably cause losses in aerodynamic performance. The specific effects may be dependent on the position and the configuration of the baffle board. Therefore, how to make a comprehensive and detailed optimization of the board parameters could become the focus of future research.

Author Contributions: Conceptualization, B.W.; methodology, B.W.; validation, B.W.; formal analysis, B.W. and S.L.; investigation, B.W.; resources, B.W.; data curation, S.L.; writing—original draft preparation, B.W.; writing—review and editing, Q.W.; visualization, B.W.; supervision, B.W. All authors have read and agreed to the published version of the manuscript.

Funding: This research received no external funding.

Institutional Review Board Statement: Not applicable.

Informed Consent Statement: Not applicable.

Data Availability Statement: The original contributions presented in the study are included in the article, further inquiries can be directed to the corresponding author.

Conflicts of Interest: The authors declare no conflicts of interest.

Nomenclature

CFD	computational fluid dynamics
DC60	a total pressure distortion index
j	complex imaginary unit
k	turbulent kinetic energy
LSA	low scattering angle
m	flow rate
MLFMM	multi-level fast multipole method
MOM	method of moment
P	static pressure
P^*	total pressure
PO	physics optics
\bar{q}	average dynamic pressure

R	distance between object and receiving system
RCS	radar cross-section
RL-GO	ray launching-geometrical optics
S	power density
SST	shear stress transfer
TPR	total pressure recovery
y+	a dimensionless distance parameter
σ	total pressure recovery (TPR) coefficient
μ	relative magnetic permeability
ϵ_r	relative dielectric constant
λ	radar wavelength
ω	dissipation rating
φ	flow coefficient

References

- Lee, C.S.; Lee, S.W.; Chou, R. RCS reduction of a cylindrical cavity by dielectric coating. In Proceedings of the IEEE International Symposium on Antennas and Propagation Digest, Philadelphia, PA, USA, 8–13 June 1986; Volume 1, pp. 305–308.
- Ding, F.; Liu, J. An overview of waverider design concept in airframe/inlet integration methodology for air-breathing hypersonic vehicles. *Acta Astronaut.* **2018**, *152*, 639–656. [\[CrossRef\]](#)
- Hall, G.R.; Hurwitz, W.M.; Tiebens, G.S.; Norby, W.P.; Singhsinsuk, P.; Wilt, C.E. *Development of the F/A-18E/F Air Induction System*; AIAA: Reston, VA, USA, 1993; pp. 93–2152.
- Asghar, A.; Stowe, R.A.; Allan, W.D.E.; Alexander, D. Entrance aspect ratio effect on S-duct inlet performance at high-subsonic flow. *J. Eng. Gas Turbines Power-Trans. ASME* **2017**, *139*, 052602. [\[CrossRef\]](#)
- Fiola, C.; Agarwal, R.K. Simulation of secondary and separated flow in a diffusing S-duct using four different turbulence models. *Aerosp. Eng.* **2014**, *228*, 1954–1963. [\[CrossRef\]](#)
- Xu, H.; Huang, W.; Du, Z. Influences of microjet pressure and number of microjets on the control of shock wave/boundary layer interaction. *Aerosp. Sci. Technol.* **2023**, *138*, 108345. [\[CrossRef\]](#)
- Shogo, O.; Manami, F.; Yusuke, H. Experimental study of high-speed air intake performance by side clearance. *Aerosp. Sci. Technol.* **2022**, *123*, 107439.
- Sun, S.; Wu, Z.; Huang, H.; Bangga, G.; Tan, H. Aerodynamic Response of a Serpentine Inlet to Horizontal Periodic Gusts. *Aerospace* **2022**, *9*, 824. [\[CrossRef\]](#)
- Pattnaik, S.P.S.; Rajan, N.K.S. Numerical investigation of impact of fixed-exit boundary-layer bleed on supersonic intake performance. *Aerosp. Sci. Technol.* **2022**, *120*, 107286. [\[CrossRef\]](#)
- Javad, S.Y.; Esmaili, S. Source of buzz instability in a supersonic air inlet. *Aerosp. Sci. Technol.* **2023**, *138*, 108334.
- Crispin, J.W., Jr.; Maffett, A.L. Estimating the radar cross section of a cavity. *IEEE Trans. Aerosp. Electron. Syst.* **1970**, *6*, 672–674. [\[CrossRef\]](#)
- Umashankar, K.; Taflove, A.; Rao, S. Electromagnetic scattering by arbitrary shaped three dimensional homogeneous lossy dielectric objects. *IEEE Trans. Antennas Propag.* **1986**, *34*, 758–766. [\[CrossRef\]](#)
- Vogel, M. Radar cross section of aircraft with engine inlets including fan blades. In Proceedings of the IEEE International Symposium on Antennas and Propagation, Fajardo, PR, USA, 26 June–1 July 2016; pp. 1369–1370.
- Chung, S.S.M.; Tuan, S.C. Efficacy of an S-shaped air inlet on the reduction of front bistatic radar cross section of a fighter engine. *Prog. Electromagn. Res. B* **2021**, *92*, 193–211. [\[CrossRef\]](#)
- Choi, W.H.; Kim, T.I.; Lee, W.J. Broadband radar absorbing sandwich composite with stable absorption performance for oblique incidence and its application to an engine duct for RCS reduction. *Adv. Compos. Mater.* **2021**, *30*, 76–90. [\[CrossRef\]](#)
- Qiang, W.; Bin, W. Numerical investigation of aerodynamic and electromagnetic performances for S-duct caret intake with boundary-layer bleed system. *Int. J. Aerosp. Eng.* **2023**, 1194655. [\[CrossRef\]](#)
- McLelland, G.; MacManus, D.G.; Zachos, P.K.; Gil-Prieto, D.; Migliorini, M. Influence of Upstream Total Pressure Profiles on S-Duct Intake Flow Distortion. *J. Propuls. Power* **2020**, *36*, 346–356. [\[CrossRef\]](#)
- Bin, W.; Qiang, W. Effect of boundary-layer bleed system on radar stealth and aerodynamic performances of S-duct caret intake. In Proceedings of the 2023 2nd International Symposium on Aerospace Engineering and Systems (ISAES), Nanjing, China, 19–21 May 2023; pp. 360–366.
- Bin, W.; Qiang, W. Numerical optimization of electromagnetic performance and aerodynamic performance for subsonic S-duct intake. *Aerospace* **2022**, *9*, 665. [\[CrossRef\]](#)
- Herrmann, C.D.; Koschel, W.W. Experimental investigation of the internal compression of a hyper-sonic intake. In Proceedings of the 38th AIAA/ASME/SAE/ASEE Joint Propulsion Conference & Exhibit, Indianapolis, Indiana, 7–July 2002; p. 4103.
- ANSYS, Inc. *Southpointe 2600 Ansys Drive*; ANSYS, Inc.: Canonsburg, PA, USA; Available online: www.ansys.com (accessed on 4 February 2020).
- Anastassiou, H.T.; Volakis, J.L. *The Mode Matching Technique for Electromagnetic Scattering by Inlets with Complex Terminations*; Radiation Laboratory, University of Michigan: Ann Arbor, MI, USA, 1993; pp. 1363–1391.

23. USA Altair Engineering Inc. East Big Beaver Road, Troy, Michigan, USA. Available online: www.altair.com.cn/feko (accessed on 28 May 2020).
24. Zeng, L.F.; Pan, D.Y.; Ye, S.J. A fast multi-objective optimization approach to S-duct scoop inlets design with both inflow and outflow. *Proc. Inst. Mech. Eng. Part G-J. Aerosp. Eng.* **2019**, *233*, 3381–3394. [[CrossRef](#)]

Disclaimer/Publisher’s Note: The statements, opinions and data contained in all publications are solely those of the individual author(s) and contributor(s) and not of MDPI and/or the editor(s). MDPI and/or the editor(s) disclaim responsibility for any injury to people or property resulting from any ideas, methods, instructions or products referred to in the content.